Original Paper

Eletrônica de Potência
Open Journal of Power Electronics

Received August 18, 2025; Received in revised form October 20, 2025; Accepted November 05, 2025; Date of publication January 06, 2026.
The review of this paper was arranged by Associate Editor Renata O. de Sousa and Editor-in-Chief Heverton A. Pereira.

Digital Object Identifier http://doi.org/10.18618/REP.e202601

Small Signal Analysis of Rotating Reference Frame Based Synchronization Control for Microgrid to Grid Changeover

Deepak Gehlot[1,2,*], Shoubhik Mukherjee[1], A.S. Krishna Priya[1], Mukesh Kr. Pathak[2]

[1] BHEL Corp.R&D, Electrical and Power Electronics Lab, Hyderabad, Telangana, India
[2] IIT Roorkee, Department of Electrical Engineering, India

e-mail: deepak_g@ee.iitr.ac.in*; sounitdgp1@gmail.com; krishnapriya.sai@gmail.com; mukesh.pathak@ee.iitr.ac.in.
*Corresponding Author.

ABSTRACT Reliable synchronization is essential for ensuring stability during the transition of microgrids between islanded and grid-connected operation, particularly in converter-dominated low-inertia systems. This paper outlines a small signal analysis for the novel synchronization control of an islanded microgrid comprising two or more parallel-connected voltage source converters. It focuses on the development of simple and effective microgrid synchronization strategies with a minimum Rate of Change of Frequency (ROCOF), enabling the integration of Distributed Energy Resources (DER) into growing low-inertia power systems. The proposed method is based on a rotating reference frame-based algorithm with two Proportional-Integrator (PI) controllers at the secondary control level, minimizing the computational complexity by reducing the number of control loops compared with conventional approaches. A small-signal model has been developed and validated using eigenvalue analysis to ensure stability during the mode transitions. The developed controls were validated on a test setup comprising of a 25 kW Grid-Forming Converter (GFC) and a 25 kW Grid-Following Converter (GFL).

KEYWORDS Current controller, Droop control, Grid following converter, Grid forming converter, Hardware in Loop controller, Phase Locked Loop

I. INTRODUCTION

In recent years, due to a rapid increase in the integration of renewable energy resources, Power systems have undergone a transitional shift from traditional centralized generation with unidirectional power flow to decentralized power architecture with bidirectional power flow. This shift has resulted in increased emphasis on the development of control strategies that can optimize the performance of Distributed Energy Resources (DERs) while improving their availability and power quality under varied grid conditions, including faults and disruptions.

A key enabler to achieve the above-stated objectives is microgrid, which is a localized system consisting of DERs such as solar photovoltaics, wind turbines, and energy storage systems, along with industrial and residential loads, within a specific electrical boundary. These Microgrids usually stay synchronized with the grid but have ability to disconnect and function independently in islanded mode during a grid disturbance.

A major challenge for Microgrids is to maintain system stability during transitions between operational modes, particularly when switching from islanded to grid-connected mode after grid restoration. In islanded mode, at least one converter uses GFC controls to manage voltage and frequency, while in grid-connected mode, all converters employ Grid-Following(GFL) controls. This transition is complicated by the shift in converter controls, which can affect synchronization.

Recent studies on synchronization control for microgrid transitions show that phase-locked loop (PLL) techniques remain the most widely adopted because of their accuracy in tracking grid frequency, phase, and voltage. Advanced second-order generalized integrator (SOGI) designs have been developed to improve performance. For example, [1] introduced a dual-enhanced SOGI vector-based method for fault-resilient grid-tied converters, while [2] proposed an improved cascaded SOGI with adaptive frequency-locked loop (FLL) gain for photovoltaic islanding synchronization. Both, however, still exhibit a high rate of change of frequency (ROCOF) and cross-coupling limitations. Earlier work by [3] used Dual Second Order Generalized Integrator (DSOGI) with a synchronous reference frame PLL, which proved reliable but slow, with synchronization times dependent on frequency differences.

Hybrid PLL/FLL approaches have aimed to improve adaptability. [4] employed an enhanced second-order complex vector filter-based FLL with dedicated loops for frequency, phase, and magnitude, while [5] proposed a universal FLL suitable for various microgrid configurations. Both methods, however, remain susceptible to high transients or suffer from implementation complexity. [6] and [7] used PLL-based theta-shift strategies that can introduce large ROCOF and load transients, and [8] combined droop control

with PLL for minimal-communication synchronization, at the cost of slower convergence in dynamic grids.

Several studies have attempted to enhance PLL robustness through filtering or estimation. [9] integrated a Kalman filter with synchro-extraction but still relied on simple theta switching, leading to transient spikes. [10] added a rate limiter to avoid abrupt changes, though its tuning is critical for weak grids. [11] used a Goertzel filter-PLL to improve harmonic rejection, yet cross-coupling effects were left unaddressed.

Droop and virtual synchronous generator (VSG) controls provide another pathway by emulating synchronous machine behavior. [12] applied active droop for phase and voltage matching, and [13] proposed a universal droop controller for resynchronization, both of which are vulnerable to instability under high ROCOF. VSG methods from [14] and [15] offered improved dynamic response but were prone to phase jumps or ignored coupling effects.

Adaptive, linearized, and non-linear control schemes have also been explored. [16] implemented an adaptive PLL for wind-solar microgrids; [17] presented a linearized robust Proportional Integrator (PI) method for GFMs; and [18] combined a non-linear PLL with droop control. While effective under certain conditions, these approaches often suffer from operational range limitations or high ROCOF during transitions.

Some researchers have focused on communication-assisted or supervisory synchronization. [19] used a controller area network (CAN) to transmit SRF-PLL phase information, but sudden theta shifts caused transients in motor-dominated loads. [20] Implemented a supervisory PLL with pulse commands, which extended synchronization time and added dependency on central control. Passive breaker-based synchronization, as in [21], can be simple but risks mismatches during rapid mode changes.

Other architectures employ multiple control loops. [22] and [23] designed three-loop schemes for frequency, voltage, and phase restoration, though sharp transients remained an issue. [24] used FM-modulated signals for islanded converter synchronization, providing noise resilience but potentially affecting voltage quality.

To reduce complexity [25], some researchers have suggested using the previous mode's last theta as a starting reference for the next mode during the GFL to GFM transition, which can lead to high ROCOF and transient currents. [26] has proposed a non-PLL-based technique. The suggested approach maintains stability during transitions but has reduced accuracy in noisy conditions.

In summary, a detailed literature survey highlights the considerable progress made in the area of microgrid synchronization; still, no single approach is without its limitations. Some of the key limitations that emerge from this discussion are that most existing approaches are based on three interlinked loops for voltage, frequency, and phase synchronization. This cross-coupling between loops results in an increase in computational requirements and synchronization time. Another major limitation is high ROCOF during islanding to grid transition, which in turn can result in activation of protection systems or damage sensitive equipment. Further synchronization controller tuning has not been addressed in totality; some literature that does address it has adopted an overly complicated approach, making it suitable for specific scenarios. Finally, stability studies of synchronization loops have limited consideration of how synchronization dynamics interact with droop or secondary control mechanisms.

The primary objective of this research is to develop a simplified and fast-response synchronization technique by implementing a two-loop synchronization control based on a rotating reference frame. The key contributions are:1) A simplified control architecture based on a rotating reference frame with minimum PI controls to minimize the nonlinearity and reduce computational requirements. 2)A comprehensive small-signal model has been formulated to examine the influence of the proposed synchronization controls on droop regulation and to assess system stability under dynamic operating conditions, 3) A novel sequential synchronization algorithm is proposed in which the phase and frequency loop (PSL) and voltage synchronization loop (VSL) are activated one by one. This, in turn, prevents cross-coupling between PSL and VSL, enabling smoother transitions.
The developed controls have been validated on a test setup consisting of one 25 kVA GFM and one 25 kVA GFL converter for both transition scenarios.

Beyond addressing the specific challenges of microgrid synchronization, the study contributes to the larger goal of improving grid stability, resilience, and adaptability with integration of converter based DERs.

The remaining part of the paper consists of five sections. Section II presents the microgrid system configuration, Section III details the proposed synchronization control design, Section IV develops the small signal model, Section V provides experimental validation, and Section VI concludes with future research directions.

II. SYSTEM CONFIGURATION

A. *SYSTEM DESCRIPTION*

This study focuses on two converters due to the unrestricted nature of the proposed approach to the number of converters. This centralised method can be utilised in a microgrid with multiple converters using low-capacity communication. Fig. 1 illustrates the Signal line of the suggested Microgrid. The setup comprises a Battery Energy Storage System (BESS), Power Conversion System (PCS) and a Solar Photovoltaic Power Conditioning unit (PCU) connected to an AC 415 V bus through CB-1 and CB-2 breakers, along with a local variable R-L load linked via CB-3. CB-4 is employed to connect the Microgrid to the primary grid.

B. *SYSTEM CONTROL ARCHITECTURE*

The BESS PCS uses droop control mode when operating in a microgrid and as a GFL converter connected to the grid. Similarly, the solar PCU operates in grid-following mode in microgrid and grid-connected operations. The droop control loop is established based on the droop characteristic of the synchronous machine, reflected in (1) and (2).

$$\omega = \omega^* - mP \quad (1)$$

$$V = V^* - nQ \quad (2)$$

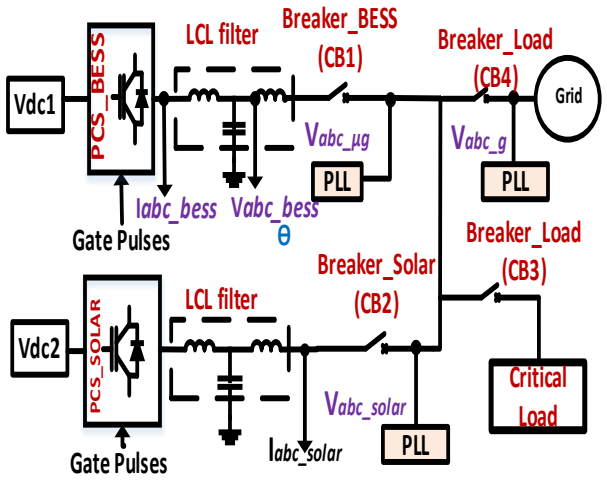

FIGURE 1. Single line diagram (SLD) of Microgrid under study.

These equations indicate a linear relationship between active power and frequency (Pf) and reactive power and Voltage (QV). The symbols ω and V represent the BESS PCS's angular frequency and voltage amplitude reference.

Meanwhile, ω* and V* denote the no-load angular frequency and voltage amplitude. P and Q are the BESS PCS output active power and reactive power, respectively, while m and n are their corresponding droop coefficients for P-ω and Q-V control. These equations yield a proportional control that enables the injected P and Q to regulate the frequency and voltage amplitude at the PCC or vice versa. The output of the droop regulator for a voltage-controlled mode VSC forms the internal converter frequency and voltage amplitude setpoints. The voltage setpoint derived from the Q droop equation is incorporated into a cascaded controller architecture consisting of an outer voltage controller loop and an inner current loop. During GFL, the BESS PCS controls include Id and Iq Current control loops. For the transition between grid-connected and islanded modes, as well as vice versa, it is suggested by [27]-[31] to employ droop control and PQ control without shared control loops or elements, which results in increased transients and control complexity.

In the proposed system control architecture during Changeover from grid-connected mode to islanding mode or islanding mode to grid-connected mode, the input to the innermost current controller only changes, while in both modes, the current control loop —which includes the feedforward of grid voltage, decoupling terms, and PI control terms—is the same, establishing appropriate control references during operation mode transitions; this, in turn, ensures minimum transients during the changeover. The overall control architecture of the system under study is shown in Fig. 2.

C. *SYNCHRONIZATION CONTROL*

In order to connect or reconnect any power source to the grid, the voltages at both ends of the point of common coupling (PCC) need to fall within the ranges specified by IEEE Standard 1547-2018[32], as outlined in Table 1.

TABLE 1. EEE1547-2018 Synchronization limits.

Aggregate Rating of DR Units (kVA)	Frequency Difference (Δf, Hz)	Voltage Difference (ΔV, %)	Phase Angle Difference (Δø, °)
0 - 500	0.3	10	20
500 – 1,500	0.2	5	15
1,500 - 10,000	0.1	3	10

However, for Power Electronics dominated microgrids limits specified by IEEE 1547-2018 may not be fully appropriate as they exhibit low inertia, limited overcurrent capacity as compared to conventional synchronous machine-based systems. For example in a 500 kW converter based microgrid with equal voltage and frequency between microgrid and grid a 10 deg phase angle deviation will result in transient current of 1.7 times rated current which can cause converter to trip or damage. This in order to achieve smooth and reliable reconnection with converter based microgrids much stringent synchronization limits are required .

III. PROPOSED SYNCHRONIZATION CONTROL DESIGN

A. *SYNCHRONIZATION FRAMEWORK*

The synchronization between the grid and microgrid is accomplished using the direct and quadrature (dq) voltage elements of the grid and the microgrid, denoted as V_{dqg} and $V_{dqµg}$. These elements are derived using the Park transformation, which leverages the phase angle of the grid voltage vectors computed by the phase-locked loop (PLL). The synchronization framework comprises a three-phase PLL to track the grid's phase angle, a low-pass filter to attenuate noise, and PI regulators for controlling the d-axis and q-axis voltage components.

To bring both sets of signals into the same dq reference frame, these values are computed for the grid reference frame, which is supposed to be more stable than the microgrid reference frame. Error Signal are determined by comparing the dq components of the grid voltage and the microgrid (µG). These error signals are then fed to a set of PI controllers. The PI controllers generate corrective signals, ΔV and Δ which are added to (1) and (2), and can be expressed mathematically as (3) and (4). These signals shift the droop operating point to achieve synchronization. When the voltage components are equivalent (Vdµg = Vdg and Vqµg = Vqg), the microgrid and grid can synchronize.

$$\omega = \omega^* - mP + \Delta\omega \qquad (3)$$

$$V = V^* - nQ + \Delta V \qquad (4)$$

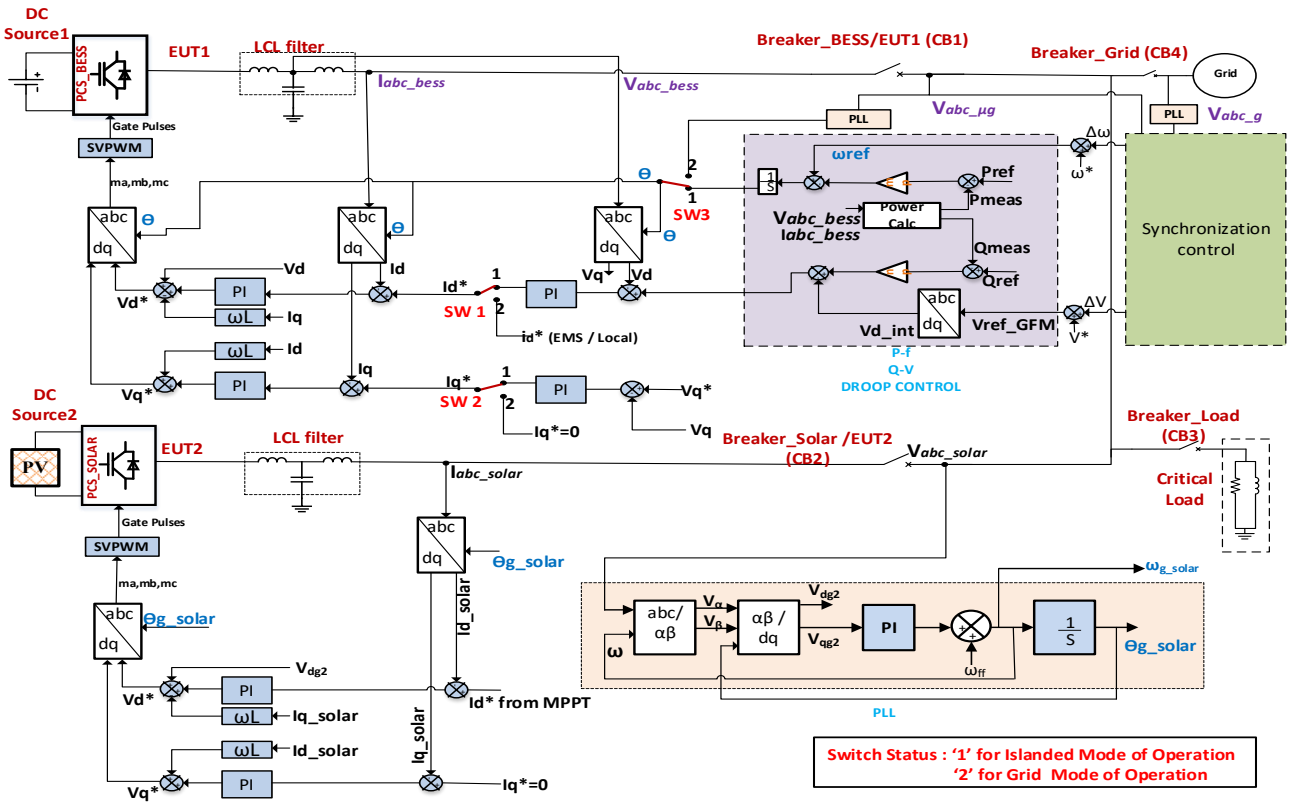

FIGURE 2. Overall control block diagram showing current, voltage and synchronization loops of the system under study

B. *SYNCHRONIZATION FRAMEWORK*

In the proposed system control architecture during Changeover from grid-connected mode to islanding mode or islanding mode to grid-connected mode, the input to the innermost current controller only changes, while in both modes, the current control loop —which includes the feedforward of grid voltage, decoupling terms, and PI control terms—is the same, establishing appropriate control references during operation mode transitions; this, in turn, ensures minimum transients during the changeover. The overall control architecture of the system under study is shown in Fig. 2.

The synchronization process establishes a smooth connection that helps reduce fluctuations in the current and ensures the stability of the system. A control loop based on a synchronous dq reference frame is proposed to achieve synchronization, as illustrated in Fig. 3. Compared to existing methods, the main difference in the proposed synchronization technique is the need for separate control loops dedicated to voltage, frequency, and phase synchronization. The latter approach involves three loops with cross-coupling, making minimizing the number of loops essential. Therefore, the presented method introduces a control architecture with the least number of control loops. This segment delineates the design of a synchronization control scheme employing droop control mechanism within a BESS PCS. The VSL, articulated in (4), leverages a Q/V droop control coefficient, denoted as n, while Q symbolizes the BESS PCS's output reactive power and V* represents the nominal output voltage corresponding to no-load condition alongside the BESS's synchronization voltage. Functioning concurrently with the Q/V droop regulator within a conventional synchronization control framework, the VSL addresses dynamic D-axis voltage discrepancies (ΔVd) via (5).

$$\Delta Vd = Vd\mu g * Cos\left((\omega\mu g - \omega g)t + (\Theta\mu g - \Theta g)\right) - Vdg * Cos\left((\omega\mu g - \omega g)t + (\Theta\mu g - \Theta g)\right) \quad (5)$$

Similarly, (6) introduces the handling of dynamic Q-axis voltage variations (ΔVq) within the PSL, signifying a direct correlation between phase/frequency adjustments and the error dynamics of both VSL and PSL.

$$\Delta Vq = Vq\mu g * Sin\left((\omega\mu g - \omega g)t + (\Theta\mu g - \Theta g)\right) - Vqg * Sin\left((\omega\mu g - \omega g)t + (\Theta\mu g - \Theta g)\right) \quad (6)$$

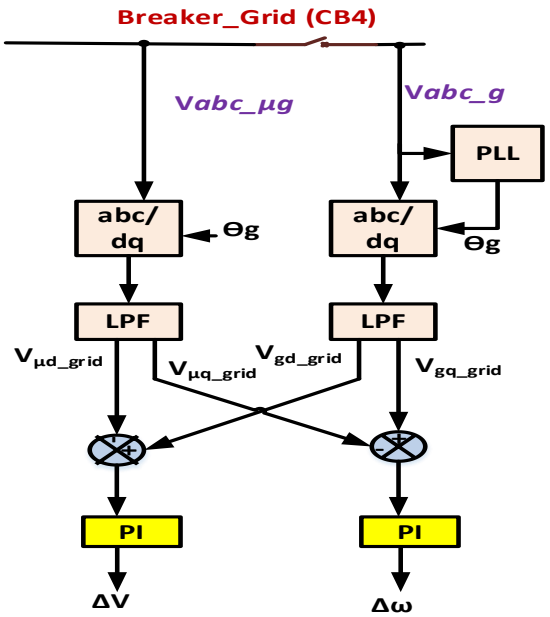

FIGURE 3. Synchronization loop control block diagram.

C. SEQUENTIAL SYNCHRONIZATION ALGORITHM

The concurrent operation of these loops could culminate in voltage oscillations and potential system instability. To mitigate such challenges, a novel algorithmic strategy depicted in Fig. 4 proposes the decoupling of PSL and VSL by initially aligning the phase angle and frequency differences to zero followed by minimizing voltage differentials. A latch time of 150 ms is kept with PSL condition, as it ensures that the maximum frequency difference between voltages is less than 0.05 Hz while maintaining phase angle difference less than 3 degrees.

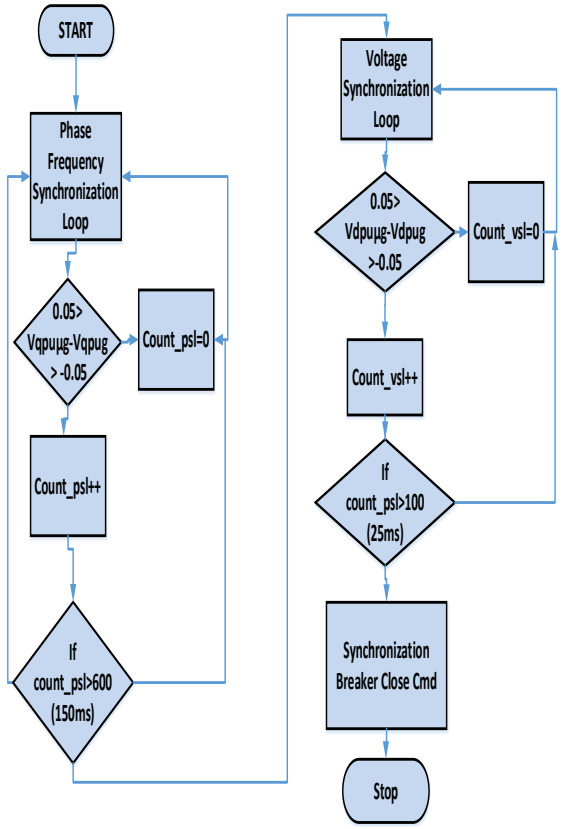

FIGURE 4. Proposed algorithm flowchart

The sequential approach prevents cross-coupling between voltage and frequency loops, which can cause oscillations when both loops operate simultaneously. During large phase differences, simultaneous operation creates interaction terms that can destabilize the system. The sequential approach ensures that:

Phase 1: Phase and frequency synchronization is achieved first ($\Delta Vq \rightarrow 0$)

Phase 2: Voltage magnitude synchronization follows ($\Delta Vd \rightarrow 0$)

Phase 3: Final verification and grid connection

D. CONTROLLER DESIGN

The synchronization controller plays a pivotal role in ensuring a smooth and stable reconnection of converter-based microgrids. Traditional PLL-based synchronization techniques often encounter challenges such as high rates of change of frequency (ROCOF) and large transient currents during switching events. To overcome these limitations, this study introduces a Phase/Frequency Synchronization Loop (PSL) designed through a systematic control methodology.

The controller is designed to meet the following operational targets:

Maximum allowable ROCOF: ≤ 1 Hz/s

Maximum phase angle deviation: ≤ 5°

Maximum voltage magnitude deviation: ≤ 3%

Target synchronization time: ≤ 1.5 seconds

Minimum damping ratio: ≥ 0.7 to suppress oscillations

Minimum phase margin: ≥ 45° to ensure stability

To satisfy these design goals, the synchronization loop is configured with a low bandwidth, balancing responsiveness and stability. The structure of the proposed Phase/Frequency Synchronization Controller is illustrated in Fig. 5.

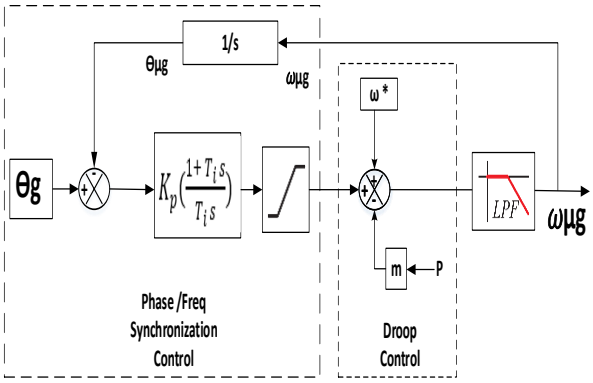

FIGURE 5. Phase frequency synchronization control

The open-loop transfer function of the PSL can be expressed as:

$$PSLtf= \frac{Kp(1+Tis)}{s} * \frac{1}{1+s\left(\frac{Ts}{2}+Tf\right)} * \frac{1}{s} \quad (7)$$

Where, Kp, Ti, Ts, and Tf represent the controller gain, integral time constant, switching period, and low-pass filter time constant, approximating the microgrid response as a first-order filter.

This configuration introduces two poles at the origin, one real pole, and one zero. Hence, the symmetrical optimum tuning method is applied to determine the optimal parameters. The calculated controller constants are as follows:

- Small time constant: a=Ts/2+Tf=0.000125+0.1=0.100125
- Integral time: Ti=4a=0.4005
- Gain: Kp=1/(2a)=4.994

To further enhance damping and limit overshoot, the final controller parameters were fine-tuned through optimization, as summarized in Table 2.

TABLE 2. Optimized Parameters for phase/frequency synchronization controller

Parameter	Value	Parameter	Value
Tf (Microgrid response approx. as Low pass)	0.1	Ts (Converter Switching Frequency)	0.00025
Ti (PSL Integral Time Constant)	2.909	Kp(PSL gain)	2.6214

Further the performance of optimized parameters with respect to calculated parameters is shown in table 3.

TABLE 3. Performance Comparison of Symmetric Optimum vs. Optimized Parameters

Metric	Symmetric Optimum	Optimized Design	Improvement
Gain (Kp)	4.994	2.6214	Reduced
Integral Time (Ti, s)	0.4005	2.909	Increased
Natural Frequency (rad/s)	4.89	2.17	55% lower
Damping Ratio (ζ)	0.45	0.85	89% higher
Rise Time (s)	0.37	0.83	Slower start
Settling Time (s)	1.93	1.28	34% faster
Overshoot (%)	19.3	0.7	96% lower
Phase Margin (°)	45	69	53% higher
Crossover Freq. (Hz)	0.794	0.301	62% lower

IV. SMALL SIGNAL MODELLING OF SYNCHRONIZATION CONTROL

In this section, the designed controller's performance and the stability of the synchronization control system are verified using a small signal model and eigenvalue analysis.

The system under consideration is represented by a set of nonlinear differential equations with state variables, inputs, and outputs to develop a state space model as in (8). The state variables are the derivatives of the system, and they describe the system's response when the present state, excitation inputs, and state equations are known.

$$\frac{dx}{dt} = f\big(x(t), u(t)\big) \ (8)$$

$$y = g(x(t), u(t)) \ (9)$$

Where y is the output vector, x(t) is the state vector, and u(t) is the input vector.

The Jacobian matrix, J, is used to linearize a given system and must be assessed at a point of operation known as the steady-state values of the differential equations. The physical system is also affected by external inputs, which must be included and linearized with the Jacobian matrix. The complete dynamic behavior of the linearly approximated system is modelled with additional matrices C and D to determine the system's outputs.

Thus, the system can be represented by (10) & (11) i.e.

$$\frac{d\Delta x}{dt} = A\Delta x + B\Delta u \ (10)$$

$$\Delta y = C\Delta x + D\Delta u \ (11)$$

$A = \Delta xf$, $B = \Delta uf$, $C = \Delta xg$, $D = \Delta ug$,

Δ denotes the small-signal deviation around the steady-state operating point. The Jacobian matrix of f pertaining to the states, x, is represented by Δxf, and the Jacobian matrix of f pertaining to the inputs, u, is represented by Δuf. The Jacobian matrix of g concerning the states, x, is represented by Δxg, and the Jacobian matrix of g pertaining to the inputs, u, is represented by Δug.

For the Synchronization Control differential equation based on system control block diagram 6 are

$$\frac{dx2}{dt} = \frac{d\theta\mu g}{dt} = x1 + Kp(\theta g - \theta\mu g) + \omega droop \ (12)$$

$$\frac{dx1}{dt} = Ki(\theta g - \theta\mu g) + \omega droop \ (13)$$

For state space representation of the above (12) & (13) is as shown in 14 & 15, inputs variables are θg, $\omega droop$, Output variable is $\omega\mu g$ and state variables are x1 i.e. Integraloutput of Phase error and $\theta\mu g$ i. e. microgrid phase angle (integral of microgrid frequency).

$$\dot{x}_1 = -k_i\theta\mu g + k_i\theta g \ (14)$$

$$\dot{x}_2 = x1 - k_p\theta\mu g + k_p\theta g + \omega droop \ (15)$$

(14) & (15) can be rewritten as (16) & (17)

$$\begin{bmatrix}\dot{x}_1\\ \dot{x}_2\end{bmatrix} = \begin{bmatrix}0 & -k_i\\ 1 & -k_p\end{bmatrix}\begin{bmatrix}x_1\\ x_2\end{bmatrix} + \begin{bmatrix}k_i & 0\\ k_p & 1\end{bmatrix}\begin{bmatrix}\theta_g\\ \omega_{droop}\end{bmatrix} \ (16)$$

$$Y = \omega\mu g = [1 \quad -k_p]\begin{bmatrix}x_1\\ x_2\end{bmatrix} + [k_p \quad 1]\begin{bmatrix}\theta_g\\ \omega_{droop}\end{bmatrix} \ (17)$$

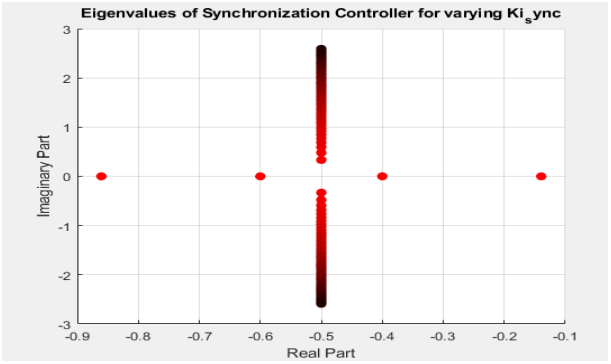

FIGURE 6. Eigen values of synchronization controller with varying values of Ki from 0.12 to 7 with Kp=1

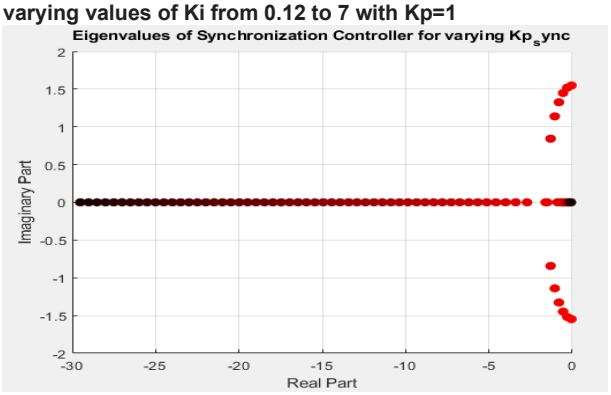

FIGURE 7. Eigen Values of Synchronization controller with varying values of Kp from 0.1 to 30 with Ki=2.4

From the eigenvalue analysis shown in Figs. 6 & 7, it can be observed that all eigenvalues lie in the left-half plane, verifying that the proposed controller values are stable for for parameter variations up to Kp = 30. Further, the selected values ensure a stable dynamics during the microgrid-to-grid transition with minimum transients on the microgrid-connected local loads.

V. EXPERIMENTAL RESULTS

To further validate the performance of the proposed algorithm for transition from microgrid to grid, an experimental test setup consisting of two 25 kVA 2-level IGBT-based converters, configurable 3-phase RL loads, and two DC sources was developed. The developed control algorithm was implemented in the Texas TMS320F28335 digital signal processor. Experimental setup is as shown in Photo 1. System parameters are as given in Table -4.

TABLE 4. System Parameters for 25 kVA Converter

Parameters	Value	Parameter	Value
fs	4 kHz	mP	8.5408
Vbase(V)	340	nQ	0.0034
Ibase(I)	50	Kpi	0.4064
ωbase	50	Kii	0.0012
Lpu	0.095718	Kpv	0.97
Cpu	0.054079	Kiv	0.0541
Rpu	0.003629	Droop filter	10 hz

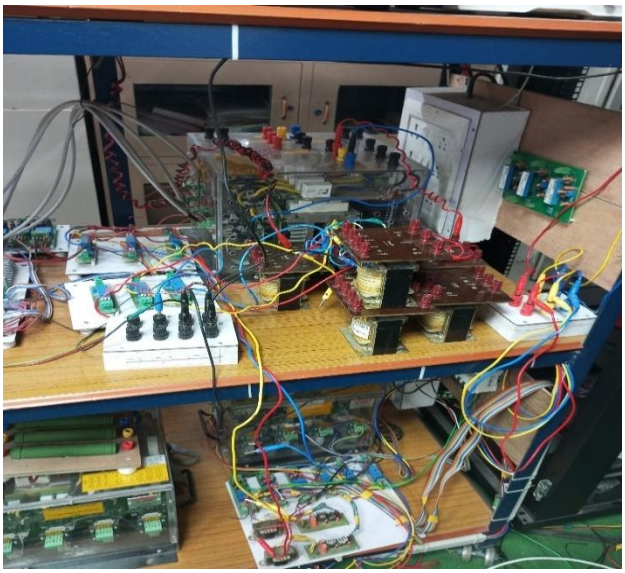

PHOTO 1: Experimental Test Setup

Initially, converter 1 (BESS), working in GFM mode, is started and loaded with a resistive load of approx. 20 kW, 6.5 kVar. Then converter 2 (Solar) is started in GFL and synchronized with converter 1 using PLL refer Fig.8. After connecting with the BESS system, the solar power generates 6.5 kW, resulting in the reduction of BESS power to 13.5 kW and 6.5 kVar. The synchronization process of the microgrid (BESS+Solar+Load) using the proposed synchronization algorithm is then initiated by the init_sync command, as shown in Fig. 9. Fig. 10 & Fig. 11 depict the time taken to achieve synchronization. Once the synchronization between the incoming grid and microgrid is achieved, the grid breaker is closed, and both the BESS and the Solar converter operate in GFL mode. Post Synchronization BESS and Solar generate approx. 6.75 kW each and Grid sources 6.5 kW 6.5 kVar refer Fig 12.

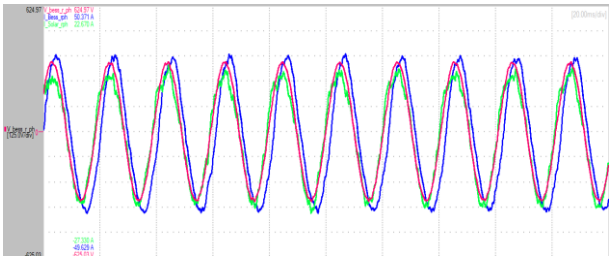

FIGURE 8. Microgrid Voltage (Red)(125V/div), BESS Current (Blue)(10A/div) and Solar Current (Green)(5A/div) with BESS and Solar operating in microgrid mode with X axis as time 20ms/div.

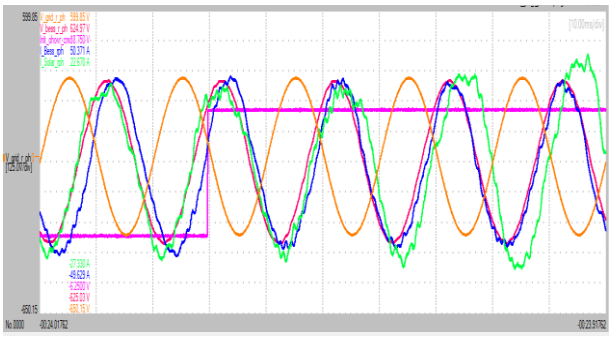

FIGURE 9. Microgrid Voltage (Red) (125V/div), Grid Voltage (Orange) (125V/div) BESS Current (Blue) (10A/div) and Solar Current (Green) (5A/div) during initialization of synchronization process (Pink) with X axis as time 10ms/div

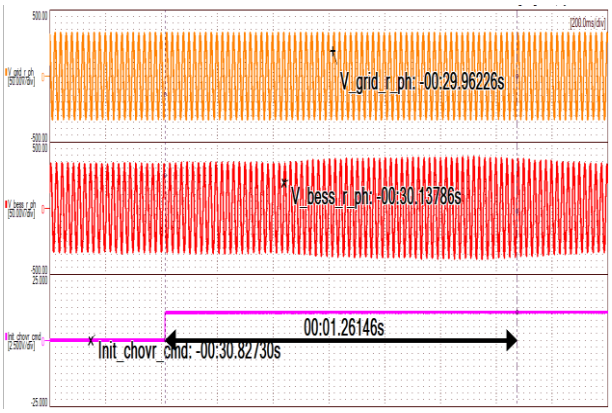

FIGURE 10. Synchronization of Microgrid Voltage (Red) (125V/div) with Grid Voltage (Orange) (125V/div) with synchronization time of 1.26 second from Init_Change_over (Blue) with X axis as time 200ms/div

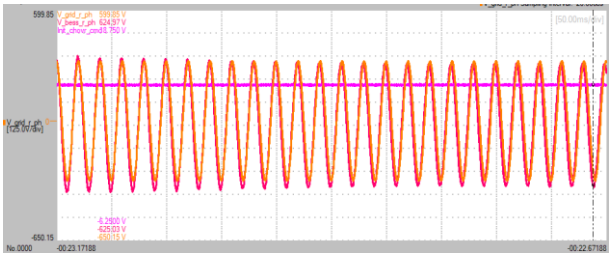

FIGURE 11. Synchronization of Microgrid Voltage (Red) (125V/div) with Grid Voltage (Orange) (125V/div) with X axis as time 50ms/div.

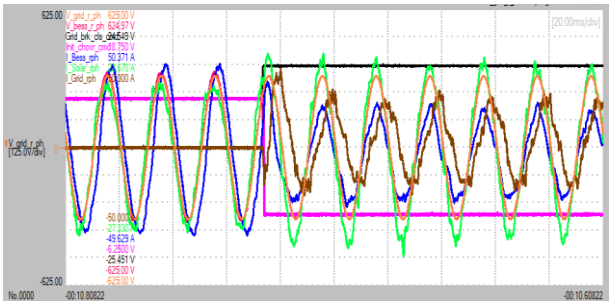

FIGURE 12. Microgrid Voltage (Red) (125V/div), Grid Voltage (Orange) (125V/div) BESS Current (Blue) (10A/div), Solar Current (Green) (5A/div) and Grid Current (Brown) (10A/div) during closure of synchronization breaker (Black) with X axis as time 20ms/div.

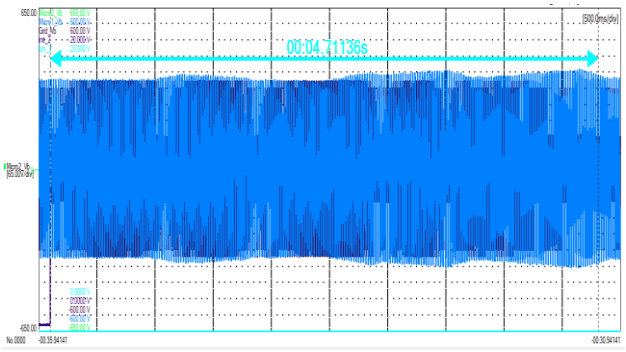

FIGURE 13. Voltage Microgrid 1(1 GFM+1GFL ,Microgrid 2(1 GFM+1 GFL) Grid pre and post Sync breaker closing with CAN communication at 1 Mbps with X axis as 500ms/div.

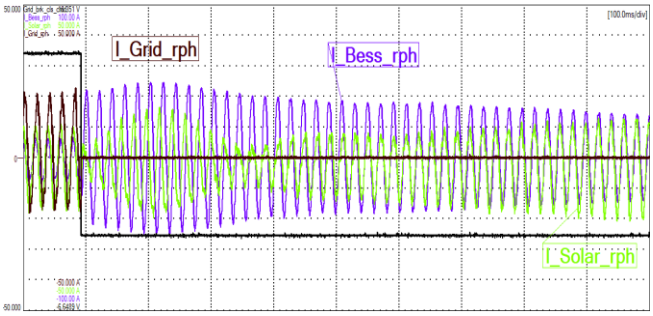

FIGURE 14. BESS Current (Blue) (10A/div), Solar Current (Green) (5A/div) and Grid Current (Brown) (10A/div) during opening of synchronization breaker (Black) with X axis as time 100ms/div.

As can be observed from Fig. 11 that a smooth transition from Microgrid to grid mode has been achieved with BESS control transitioning from GFM to GFL. Further, as shown in Fig. 9 & 10 with Grid and microgrid voltage out of phase the synchronization is achieved within 1.26 sec which further validates the performance of developed algorithm than compared to approaches presented in [33]-[35] with the maximum transient current of approx. 16%. Figure 13 shows performance of developed controls with multiple converter (4 converter 2 GFM and 2 GFL) communicating over CAN bus at 0.2 mbps being synchronized with Incoming grid wherein it takes 4.75 seconds for achieving synchronization . Figure 14 System current i.e. BESS ,Solar and Grid currents during changeover from grid to islanded.

VI. CONCLUSION

This paper introduces a novel synchronization control strategy utilizing a two-loop approach for transitions between microgrids and the main grid, achieving a synchronization time of 1.26 seconds and a transient current of 16%. Additionally, it investigates the small-signal modelling and stability of the proposed synchronisation controller, which is designed for the seamless synchronisation and reconnection of an independent microgrid with the main grid. The presented approach leverages the synchronous reference frame conversion to facilitate a smooth synchronization process before reconnection while minimizing the computational demands on controller.

The performance of the synchronization controller is influenced by the rate of change of frequency (ROCOF) that appears when a phase difference exists between the microgrid and the main grid. This relationship creates a practical limitation on how wide the controller bandwidth can be set, as a very high bandwidth may worsen transient behavior. Experimental results validate that the proposed control method results in a well-damped reconnection during synchronization.

As compared to earlier works [33]–[35], the present approach shows roughly a 20% improvement in synchronization time and about a 16% reduction in current transients. These improvements mainly result from using a simplified two-loop configuration, which avoids much of the coupling that typically occurs in the conventional three-loop PLL-based schemes. The lower bandwidth design for the PI regulators also contributes to reducing ROCOF effects, helping the microgrid maintain voltage and current stability during transition periods.

Overall, the experimental findings show that the developed method offers strong potential for practical use in low-inertia, converter-based power systems where synchronization must remain both reliable and fast. It is worth noting, however, that the present design is not suitable for synchronization of a grid-forming converter operating with an existing microgrid. Future works will focus on this aspect as well as the improving system performance during grid faults and with nonlinear loads.

AUTHOR'S CONTRIBUTIONS

D.GEHLOT: Conceptualization, Investigation, Methodology, Validation, Writing – Original Draft. **S.MUKHERJEE:** Investigation, Methodology. **A.S.K.PRIYA:** Investigation, Methodology. **M.K.PATHAK:** Conceptualization, Supervision, Writing – Review & Editing.

PLAGIARISM POLICY

This article was submitted to the similarity system provided by Crossref and powered by iThenticate – Similarity Check.

DATA AVAILABILITY

The data used in this research is available in the body of the document.

REFERENCES

[1] A. Nigam and D. Lee, "Enhanced seamless transition control of grid-tied converters using dual-eSOGI vector-based synchronization under grid faults," IEEE Trans. Power Electronics, vol. 40, no. 9, pp. 13952-13964, Sept. 2025.doi: 10.1109/TPEL.2025.3569088

[2] G. Modi and B. Singh, "Improved cascaded SOGI control for islanding-synchronization in photovoltaic system," IEEE Trans. Ind. Appl., vol. 58, no. 6, pp. 6909–6919, Nov.–Dec. 2022.doi: 10.1109/TIA.2022.3201808.

[3] M. Rizo, F. Huerta, E. Bueno, and M. Liserre, "A synchronization technique for microgrid reclosing after islanding operation," in Proc. Annu. Conf. IEEE Ind. Electron. Soc. (IECON), Oct. 2012, pp. 5596–5601.doi: 10.1109/IECON.2012.6389010

[4] A. A. Nanda, V. Narayanan, and B. Singh, "An ESOCVF-FLL based frequency adaptive two loop control scheme for seamless transition of microgrid under weak grid conditions," IEEE Trans. Consum. Electron., vol. 71, no. 1, pp. 1877–1888, Feb. 2025.doi: 10.1109/TCE.2024.3412714

[5] H. Laaksonen, "Universal grid-forming method for future power systems," IEEE Access, vol. 10, pp. 133109–133125, 2022.doi: 10.1109/ACCESS.2022.3231479

[6] B. Singh, G. Pathak, and B. K. Panigrahi, "Seamless transfer of renewable-based microgrid between utility grid and diesel generator," IEEE Trans. Power Electron., vol. 33, no. 10, pp. 8427–8437, Oct. 2018.doi: 10.1109/TPEL.2017.2778104

[7] T.-V. Tran, T.-W. Chun, H.-H. Lee, H.-G. Kim, and E.-C. Nho, "PLL based seamless transfer control between grid-connected and islanding modes in grid-connected inverters," IEEE Trans. Power Electron., vol. 29, no. 10, pp. 5218–5228, Oct. 2013.doi: 10.1109/TPEL.2013.2290059.

[8] C.-T. Lee, R.-P. Jiang, and P.-T. Cheng, "A grid synchronization method for droop controlled distributed energy resources converters," in Proc. IEEE Energy Convers. Congr. Expo. (ECCE), Phoenix, AZ, USA, 2011, pp. 743–749.doi: 10.1109/ECCE.2011.6063844

[9] P. Buduma, M. K. Das, R. T. Naayagi, S. Mishra, and G. Panda, "Seamless operation of master–slave organized AC microgrid with robust control, islanding detection, and grid synchronization," IEEE Trans. Ind. Appl., vol. 58, no. 5, pp. 6724–6738, Sep.–Oct. 2022.doi: 10.1109/TIA.2022.3185575.

[10] G. G. Talapur, H. M. Suryawanshi, L. Xu, and A. B. Shitole, "A reliable microgrid with seamless transition between grid connected and islanded mode for residential community with enhanced power quality," IEEE Trans. Ind. Appl., vol. 54(5), pp. 5246–5255, Sep./Oct. 2018.doi: 10.1109/TIA.2018.2808482

[11] Z. Zeng and W. Shao, "Reconnection of micro-grid from islanded mode to grid-connected mode used sliding Goertzel transform based filter," IET Renew. Power Gener., vol. 11, no. 7, pp. 1041–1048, May 2017.doi: 10.1049/iet-rpg.2016.0932.

[12] S. Chakraborty, M. T. Rana, and M. V. Salapka, "Active synchronization of islanded microgrid using droop-controlled grid-forming inverters," in Proc. IEEE Ind. Electron. Conf. (IECON), Brussels, Belgium, 2022, pp. 1–6. doi: 10.1109/IECON49645.2022.9968775

[13] M. Amin and Q.-C. Zhong, "Resynchronization of distributed generation based on the universal droop controller for seamless transfer between operation modes," IEEE Trans. Ind. Electron., vol. 67, no. 9, pp. 7574–7582, Sep. 2020.doi: 10.1109/TIE.2019.2942556.

[14] A. Malkhandi, T. Chakraborty, and G. Alian, "A synchronizing strategy for seamless interconnection of an isolated microgrid," in Proc. IEEE Sustain. Power Energy Conf. (iSPEC), Perth, Australia, 2022, pp. 1–5.doi : 10.1109/iSPEC54162.2022.10033025.

[15] M. Ramezani, S. Li, F. Musavi, and S. Golestan, "Seamless transition of synchronous inverters using synchronizing virtual torque and flux linkage," IEEE Trans. Ind. Electron., vol. 67, no. 1, pp. 319–328, Jan. 2019.doi: 10.1109/TIE.2019.2892697.

[16] B. Singh and S. Das, "Adaptive control for undisturbed functioning and smooth mode transition in utility-interactive wind–solar based AC/DC microgrid," IEEE Trans. Power Electron., vol. 39, no. 11, pp. 15011–15020, Nov. 2024.doi: 10.1109/TPEL.2024.3422405

[17] O. Atmaca and M. Karabacak, "Frequency, phase, and magnitude difference locked-loop based linear synchronization scheme for islanded inverters and microgrids," IEEE Access, vol. 11, pp. 61748–61772, 2023.doi:10.1109/ACCESS.2023.3287146.

[18] Youssef Hennane, Abdelmajid Berdai, Serge Pierfederici, Farid Meibody-Tabar, Jean-Philippe Martin,"Novel non-linear control for synchronization and power sharing in islanded and grid-connected mesh microgrids,"Electric Power Systems Research,Vol 208, 2022,doi: 10.1016/j.epsr.2022.107869

[19] S.S.Thale and V.Agarwal, "Controller area network assisted grid synchronization of a microgrid with renewable energy sources and storage," IEEE Transaction on Smart Grid, vol. 7, no. 3, pp. 1442–1452, May 2016.doi: 10.1109/TSG.2015.2498859

[20] J. Zapata, G. Postiglione, and F. Pezet, "Supervision based smart microgrid systems: Grid connected, island mode and seamless transition," in Proc. Int. Symp. Power Electron., Electr. Drives, Automat. Motion (SPEEDAM), Sorrento, Italy, 2020, pp. 336–341.doi: 10.1109/SPEEDAM48782.2020.9161968

[21] D. Das, G. Gurrala, and U. J. Shenoy, "Transition between grid-connected mode and islanded mode in VSI-fed microgrids," Sadhana, vol. 42, no. 8, pp. 1239–1250, Aug. 2017.doi: 10.1007/s12046-017-0659-z

[22] A. Vukojevic and S. Lukic, "Microgrid protection and control schemes for seamless transition to island and grid synchronization," IEEE Trans. Smart Grid, vol. 11, no. 4, pp. 2845–2855, Jul. 2020.doi: 10.1109/TSG.2020.2975850

[23] A. Micallef, M. Apap, C. S. Staines, and J. M. Guerrero, "Single-phase microgrid with seamless transition capabilities between modes of operation," IEEE Trans. Smart Grid, vol. 6, no. 6, pp. 2736–2745, Nov. 2015.doi:10.1109/TSG.2015.2444912.

[24] I. Patrao, R. González-Medina, S. Marzal, G. Garcerá, and E. Figueres, "Synchronization of power inverters in islanded microgrids using an FM-modulated signal," IEEE Trans. Smart Grid, vol. 8, no. 1, pp. 503–510, Jan. 2017.doi:10.1109/TSG.2016.2574038,

[25] X. Gao, D. Zhou, A. Anvari-Moghaddam, and F. Blaabjerg, "Seamless switching method between grid-following and grid-forming control for renewable energy conversion systems," IEEE Trans. Ind. Appl., vol. 61, no. 1, pp. 597–606, Jan.–Feb. 2024. doi:10.1109/TIA.2024.3471728

[26] J. Wang, B. Lundstrom, and A. Bernstein, "Design of a non-PLL grid-forming inverter for smooth microgrid transition operation," in Proc. IEEE Power Energy Soc. Gen. Meeting (PESGM), Montreal, Canada, 2020, pp. 1–5.doi: 10.1109/PESGM41954.2020.9282077

[27] Irvin J. Balaguer; Qin Lei; Shuitao Yang; Uthane Supatti; Fang Zheng Peng "Control for Grid-Connected and Intentional Islanding Operations of Distributed Power Generation" in IEEE Transactions on Industrial Electronics , Volume: 58, Issue: 1, pp. 147-157, January 2011).doi: 10.1109/TIE.2010.2049709

[28] Thanh-Vu Tran; Tae-Won Chun; Hong-Hee Lee; Heung-Geun Kim; Eui-Cheol Nho "PLL-Based Seamless Transfer Control Between Grid-Connected and Islanding Modes in Grid-Connected Inverters" in IEEE Transactions on Power Electronics ,Volume: 29, Issue: 10, October 2014.doi: 10.1109/TPEL.2013.229005

[29] Alves, A.G.P., Dias, R.F.S. & Rolim, L.G.B. A Smooth Synchronization Methodology for the Reconnection of Autonomous Microgrids. J Control Autom Electr Syst 31,2020, 665–674 ..doi: 10.1007/s40313-020-00636

[30] Balaguer-Alvarez, I.J.; Supatti, U.; Rivera, J.G.C.; Peng, F.Z. "Seamless Transitions between Grid-Connected and Stand-Alone Operations of Distributed Generation in Microgrids". Int. J. Eng. Res. Dev. 2014,

[31] Qinfei, S.; Guerrero, J.M.; Jing, T.; Vasquez, J.C.; Yang, R. An islanding detection method by using frequency positive feedback based on FLL for single-phase Microgrid. IEEE Transaction on. Smart Grid, 8, 1821–1830. 2015.doi: 10.1109/TSG.2015.2508813

[32] 1547-2018 - IEEE Standard for Interconnection and Interoperability of Distributed Energy Resources with Associated Electric Power Systems Interfaces. doi: 10.1109/IEEESTD.2018.8353526.

[33] Papadimitriou, C. N., Kleftakis V. A., & Hatziargyriou , N.D. ".Control strategy for seamless transition from islanded to interconnected operation mode of microgrids." Journal of Modern Power Systems and Clean Energy, 5(2), 2017.doi : 10.1007/s40565-016-0229-0

[34] Chakraborty, Soham. ,2023 "Robust Dynamic Resilient Power Grids Enabled By Modern Control Framework" Ph.D. dissertation ,University of Minnesota.

[35] Du, Y., Tu, H., & Lukic, S.. "Distributed control strategy to achieve synchronized operation of an islandedMG IEEE Transactions on Smart Grid " Vol: 10, Issue: 4, July 2019.doi: 10.1109/TSG.2018.2861679

BIOGRAPHIES

Deepak Gehlot is an electrical engineering graduate with two decades of experience in BHEL across power plant operations and power electronics technologies.
His work focuses on grid-connected converters, traction propulsion systems, energy storage applications etc.
His professional interests include converter design, control algorithms, and high-power system applications..
Deepak is currently pursuing Ph.D. (External) at IIT Roorkee.

Shoubik Mukherjee is an ECE graduate with 17 years of experience at BHEL in embedded control, FPGA development, and power electronics engineering. He has worked on advanced converter controls, real-time digital platforms, and high-performance power electronic systems. His areas of expertise include FPGA architectures, embedded software, and digital control algorithms. Shoubik is currently a Ph.D. scholar (External) at IIT Hyderabad.

A. S. Krishna Priya holds a Bachelor's degree in Electrical and Electronics Engineering and a Master's degree in Electrical Engineering. She has 17 years of experience at BHEL Corporate R&D specializing in power electronics converter design and control. Her work includes grid-connected

inverters, traction electrics, active power filters, and advanced control software development.

Mukesh Kumar Pathak received his B.E. from L.D. Engineering College, Ahmedabad, in 1986, and his M.Tech. and Ph.D. from IIT Delhi in 1995 and 2006. He previously served at NIT Hamirpur and NIT Kurukshetra before joining the Electrical Engineering Department at IIT Roorkee in 2007, where he is now a Professor. His research focuses on solar PV and EV converters, electric drive control, three-phase and multiphase motor drives, smart grids, microgrids, and solid-state transformers.